UNIVERSITY OF BIRMINGHAM

Three Hot-Jupiters on the upper edge of the mass-radius distribution

Turner, Oliver D.; Anderson, D. R.; Barkaoui, K.; Bouchy, F.; Benkhaldoun, Z.; Brown, D. J. A.; Burdanov, A.; Cameron, A. Collier; Ducrot, E.; Gillon, M.; Hellier, C.; Jehin, E.; Lendl, M.; Maxted, P. F. L.; Nielsen, L. D.; Pepe, F.; Pollacco, D.; Pozuelos, F. J.; Queloz, D.; Segransan, D.

Document Version
Publisher's PDF, also known as Version of record

[Link to publication on Research at Birmingham portal](#)

Three hot-Jupiters on the upper edge of the mass–radius distribution: WASP-177, WASP-181, and WASP-183

Oliver D. Turner [1]★ D. R. Anderson [2] K. Barkaoui,[3,4] F. Bouchy,[1] Z. Benkhaldoun,[4]
D. J. A. Brown [5,6] A. Burdanov,[3] A. Collier Cameron [7] E. Ducrot,[3] M. Gillon,[3]
C. Hellier,[2] E. Jehin,[3] M. Lendl [1,8] P. F. L. Maxted,[2] L. D. Nielsen,[1] F. Pepe,[1]
D. Pollacco,[5,6] F. J. Pozuelos,[3] D. Queloz,[1,9] D. Ségransan,[1] B. Smalley [2]
A. H. M. J. Triaud,[10] S. Udry[1] and R. G. West [5,6]

[1]*Observatoire de Genève, Université de Genève, 51 Chemin des Maillettes, CH-1290 Sauverny, Switzerland*
[2]*Astrophysics Group, Keele University, Staffordshire ST5 5BG, UK*
[3]*Space sciences, Technologies and Astrophysics Research (STAR) Institute, Université de Liège, Liège 1, Belgium*
[4]*Oukaimeden Observatory, High Energy Physics and Astrophysics Laboratory, Cadi Ayyad University, Marrakech, Morocco*
[5]*Department of Physics, University of Warwick, Coventry CV4 7AL, UK*
[6]*Centre for Exoplanets and Habitability, University of Warwick, Gibbet Hill Road, Coventry CV4 7AL, UK*
[7]*SUPA, School of Physics and Astronomy, University of St. Andrews, North Haugh, Fife KY16 9SS, UK*
[8]*Space Research Institute, Austrian Academy of Sciences, Schmiedlstr. 6, A-8042 Graz, Austria*
[9]*Cavendish Laboratory, J J Thomson Avenue, Cambridge CB3 0HE, UK*
[10]*School of Physics & Astronomy, University of Birmingham, Edgbaston, Birmingham B15 2TT, UK*

ABSTRACT

We present the discovery of three transiting planets from the WASP survey, two hot-Jupiters: WASP-177 b ($\sim$0.5 M_{Jup}, $\sim$1.6 R_{Jup}) in a 3.07-d orbit of a $V = 12.6$ K2 star, WASP-183 b ($\sim$0.5 M_{Jup}, $\sim$1.5 R_{Jup}) in a 4.11-d orbit of a $V = 12.8$ G9/K0 star; and one hot-Saturn planet WASP-181 b ($\sim$0.3 M_{Jup}, $\sim$1.2 R_{Jup}) in a 4.52-d orbit of a $V = 12.9$ G2 star. Each planet is close to the upper bound of mass–radius space and has a scaled semimajor axis, a/R_*, between 9.6 and 12.1. These lie in the transition between systems that tend to be in orbits that are well aligned with their host-star's spin and those that show a higher dispersion.

Key words: planets and satellites: detection – planets and satellites: individual: WASP-177b – planets and satellites: individual: WASP-181b – planets and satellites: individual: WASP-183b.

1 INTRODUCTION

Since the beginning of the project the Wide Angle Search for Planets (WASP; Pollacco et al. 2006) survey has discovered nearly 190 transiting, close-in, giant exoplanets. As they transit their host stars their bulk properties, mass and radius, can be determined relatively easily. Their transits allow for deeper characterization that has led to the discovery of multiple chemical and molecular species in their atmospheres (Birkby et al. 2013; de Kok et al. 2013; Wyttenbach et al. 2017; Hoeijmakers et al. 2018) and the observation of planetary winds (Brogi et al. 2016).

Close-in exoplanets can also provide information on the formation and migration mechanisms of Solar systems. It is expected that hot-Jupiter exoplanets initially form much further from their stars than where we detect them today. Therefore some mechanism must cause this migration. There are two proposed pathways,

high eccentricity migration, or disc migration. In the former some mechanism e.g. Kozai cycles (Wu & Murray 2003; Armitage 2013) or planet–planet scattering (Rasio & Ford 1996; Weidenschilling & Marzari 1996), forces the cold Jupiter into a highly eccentric orbit which then is tidally circularized via interaction with the star. During this kind of migration it is possible for the planet orbital axis to become mis-aligned with the stellar spin axis (Fabrycky & Tremaine 2007). In the latter mechanism the planet loses angular momentum via interaction with the stellar disc during formation and migrates inward (Goldreich & Tremaine 1980). This is expected to preserve the initial spin–orbit alignment (Marzari & Nelson 2009), though work is being done to investigate the production of mis-aligned planets due to inclined protoplanetary discs (Xiang-Gruess & Kroupa 2017).

The alignment between the stellar rotation axis and planet orbit can be investigated with the Rossiter–McLaughlin (RM) technique (McLaughlin 1924; Rossiter 1924; Triaud et al. 2010, etc.). These observations have shown a general trend for systems orbiting cool stars (with $T_{eff} < 6250$ K; Albrecht et al. 2012; Anderson et al.

2015b) to be more well aligned than systems orbiting hotter stars. Tides are also expected to play a role. In cool star systems, those with smaller scaled semimajor axes, a/R_*, tend to be more often well aligned than those with larger a/R_*. Though this picture is far from clear as there seems to be evidence for the hot/cool alignment disparity holding even for systems with large separations or low-mass planets meaning tidal effects should be minimal (Mazeh et al. 2015) casting tidal realignment into doubt (see also the discussion of Dai & Winn 2017).

In this paper, we present the discovery of three systems at the upper edge of the mass–radius envelop of hot giants that could be useful probes of tidal re-alignment.

2 OBSERVATIONS

Each of these planets was initially flagged as a candidate in data taken with both WASP arrays located at Roque de los Muchachos Observatory on La Palma and at the South African Astronomical Observatory (SAAO). The data were searched for periodic signals using a BLS method as per Collier Cameron et al. (2006, 2007). The survey itself is described in more detail by Pollacco et al. (2006).

In order to confirm the planetary nature of the signals radial velocity (RV) data were obtained with the CORALIE spectrograph on the 1.2-m Swiss telescope at La Silla, Chile (Queloz et al. 2000). Additional photometry was acquired using EulerCam (Lendl et al. 2012, also on the 1.2-m Swiss) and the two 0.6-m TRAPPIST telescopes (Gillon et al. 2011; Jehin et al. 2011), based at La Silla and Oukaimeden Observatory in Morocco (Gillon et al. 2017; Barkaoui et al. 2018).

Due to the low masses of WASP-181 b and WASP-183 b, we also acquired HARPS data (Pepe et al. 2002).[1] These observations are summarized in Table 1. The TRAPPIST data from 2018-08-13 contain a meridian flip at BJD $= 2458344.5639$. During analysis the data were partitioned at this point and modelled as two data sets.

Figs 1, 2, and 3 show the phase folded discovery and follow-up data. The RVs exhibit signals in phase with those found in the transit data and are consistent with companion objects of planetary mass. We checked for correlation between the RV variation and the bisector spans, see Fig. 4. We find no strong correlation and so further exclude the possibility that these objects are transit mimics. All of the data on these objects can be found in the online only tables. Examples of the layout of these tables are found in Tables A1–A4.

3 ANALYSIS

3.1 Stellar parameters

To obtain the stellar parameters effective temperature, T_{eff}, metallicity, [Fe/H], and surface gravity, $\log g$, we followed the method of Giles et al. (2018a,b) using iSpec (Blanco-Cuaresma et al. 2014b). To do this we corrected each spectrum for the computed RV shift, cleaned them of cosmic ray strikes and convolved them to a spectral resolution, R, of 47 000. Then, ignoring areas typically affected by telluric lines we used the synthetic spectral fitting technique to derive the stellar parameters. Via iSpec we used SPECTRUM (Gray & Corbally 1994) as the radiative transfer code with atomic data from VALD (Kupka, Dubernet & VAMDC Collaboration

Table 1. Observations of WASP-177, WASP-181, and WASP-183.

Date	Source	N.Obs. Filter
WASP-177		
2008 Jul–2010 Oct	WASP (North)	16 169
2008 Jun–2009 Oct	WASP (South)	10 825
2016 Aug–2018 Sep	CORALIE	26
2017 Jul 25	TRAPPIST-North	I + z
2017 Oct 19	EulerCam	B
2018 Jul 13	EulerCam	V
2018 Aug 13	TRAPPIST-North[a]	I + z
WASP-181		
2008 Sep–2010 Dec	WASP (North)	12 938
2008 Jul–2009 Aug	WASP (South)	9 059
2016 Jan–2017 Dec	CORALIE	31
2018 Oct–2019 Jan	HARPS	7
2016 Dec 06	TRAPPIST-South	I + z
2017 Jul 29	TRAPPIST-North	I + z
2017 Sep 03	EulerCam	I_c
WASP-183		
2008 Feb–2011 Mar	WASP (North)	13 733
2009 Jan–2010 May	WASP (South)	10 789
2015 May–2018 Jul	CORALIE	16
2018 Mar	HARPS	4
2018 Feb 24	TRAPPIST-North	I + z

[a]These observations were made as part of the programs Anderson:0100.C-0847(A) and Nielsen:0102.C-0414(A).

2011), a line selection based on an $R \sim 47\,000$ solar spectrum (Blanco-Cuaresma et al. 2016, 2017) and the MARCS model atmospheres. Gustafsson et al. (2008) in the wavelength range 480–680 nm. We increased the uncertainties in these parameters by adding the dispersion found by analysing the *Gaia* benchmark stars with iSpec as per Blanco-Cuaresma et al. (2014a), Jofré et al. (2014), and Heiter et al. (2015).

We determined the stellar density from an initial fit to the light curves and then used it along with the T_{eff} and metallicity to determine stellar masses, for later use in the joint analysis, and the stellar ages with the Bayesian stellar evolution code BAGEMASS (Maxted, Serenelli & Southworth 2015). The resulting parameters are presented in the top part of Table 3 and the corresponding isochrons/evolutionary tracks are shown in Fig 5.

BAGEMASS uses an MCMC with a densely sampled grid of stellar models to compute stellar masses and ages. There are three usable grids with differing mixing length parameters, α_{MLT}, and helium enhancement. The default values of these are $\alpha_{MLT} = 1.78$ and no He-enhancement. We used the BAGEMASS default parameters to model WASP-177 and WASP-181 but found that they did not fit WASP-183 very well. This is likely because WASP-183 is among the ~ 3 per cent of the K-dwarf population that are larger than models would predict (Spada et al. 2013). To account for this we follow the method of Maxted et al. (2015) in the case of Qatar-2 and use a grid provided by BAGEMASS with $\alpha_{MLT} = 1.5$. This results in a much improved fit to the observed density and temperature. We find that the resulting mass estimate is unaffected.

3.2 System parameters

To determine the system parameters we modelled the discovery and follow-up data together using the most recent version of the Markov Chain Monte Carlo (MCMC) code described in detail in

---

[1]These observations were made as part of the programs Anderson:0100.C-0847(A) and Nielsen:0102.C-0414(A).
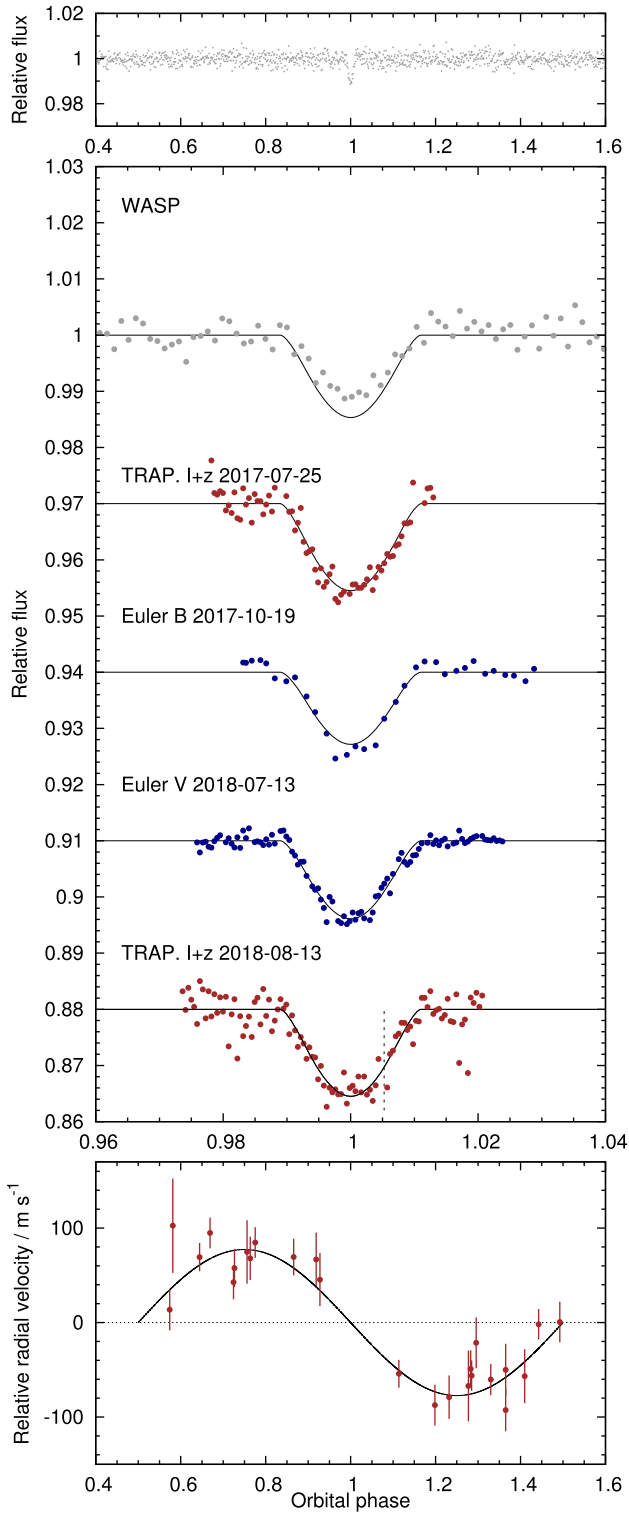
Figure 1. Data for the WASP-177 system. *Top*: WASP discovery light curve phase-folded on period found by joint analysis and binned to 2 min. *Middle*: Light curves used in joint analysis. The WASP light curve has been binned to 5 min, the others to 2, and overplotted with the transit model. Grey points are from WASP, the other data are labelled. In the online figure red points are from Eulercam and blue points from TRAPPIST. The meridian flip in the TRAPPIST data is denoted by a grey, dashed line. *Bottom*: CORALIE radial velocities used in the joint analysis overplotted with resulting model.
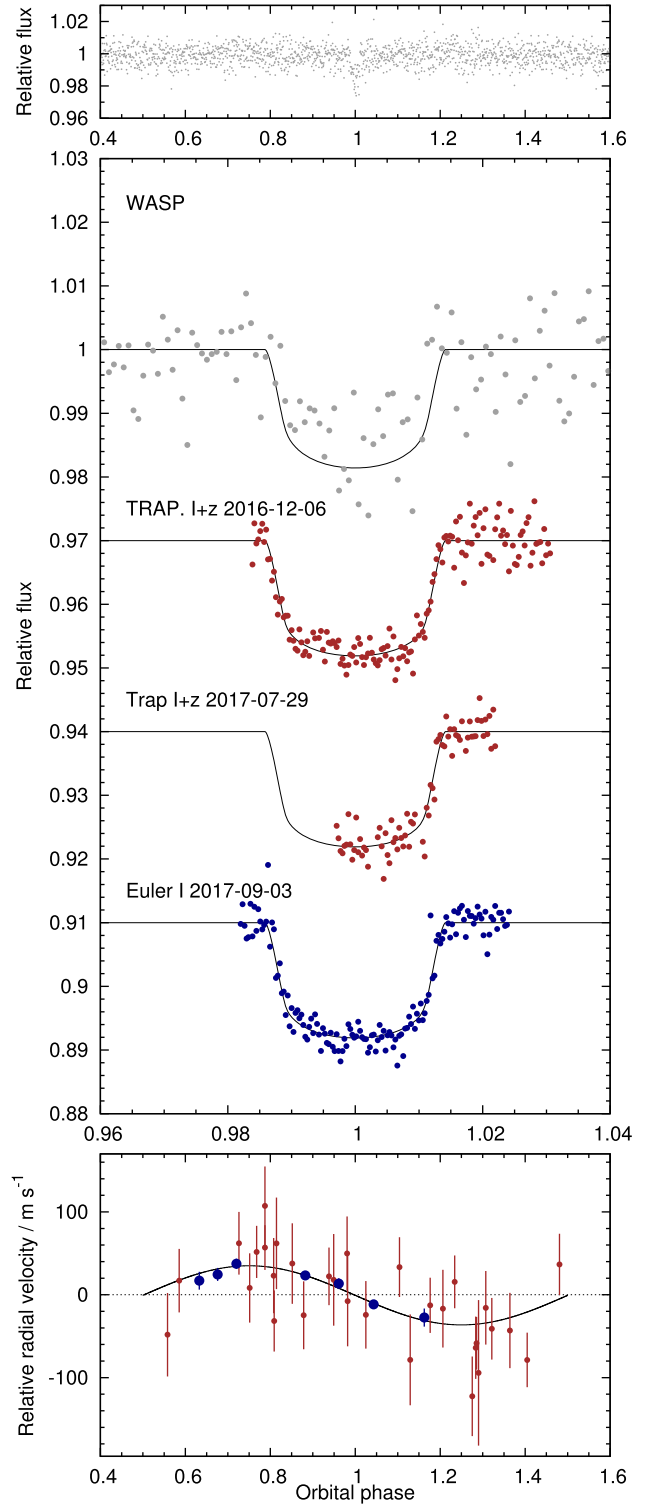
Figure 2. As for Fig. 1 for the WASP-181 system. CORALIE data in bottom figure are small (red) while HARPS data are larger (blue) symbols.
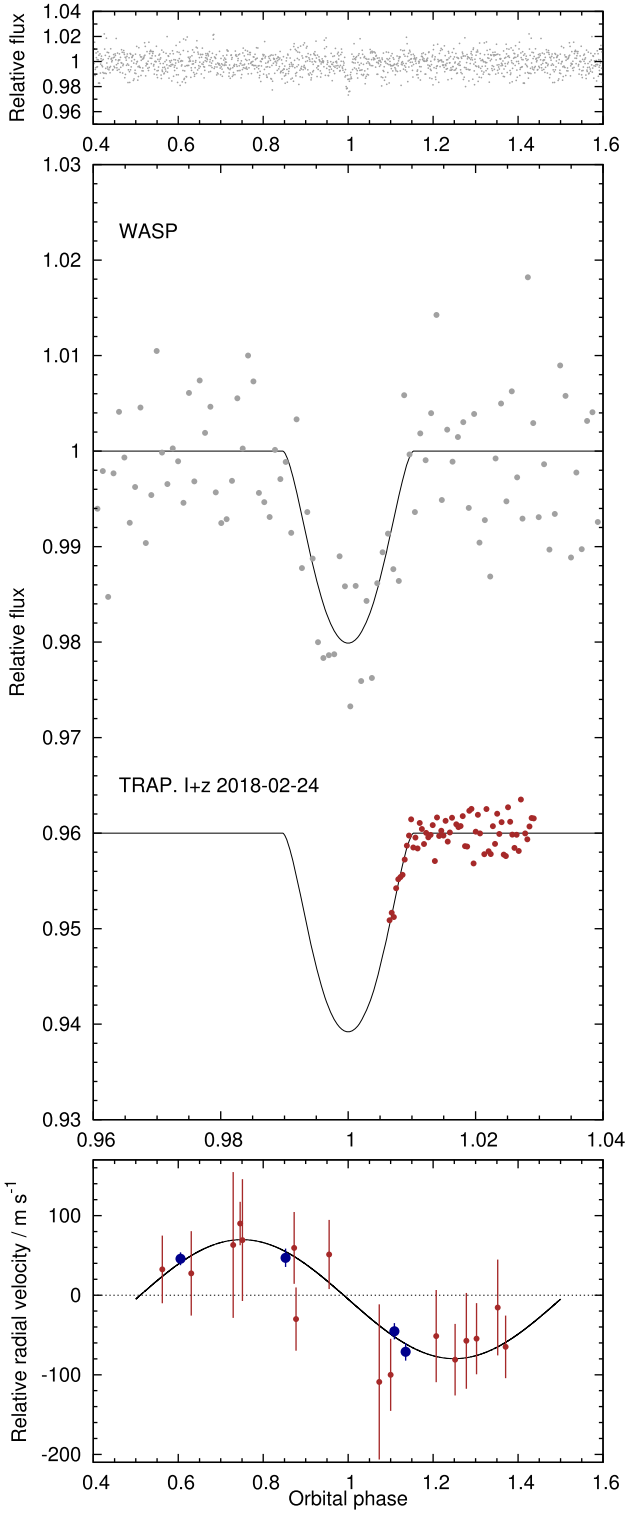
Figure 3. As for Fig. 2 for the WASP-183 system.
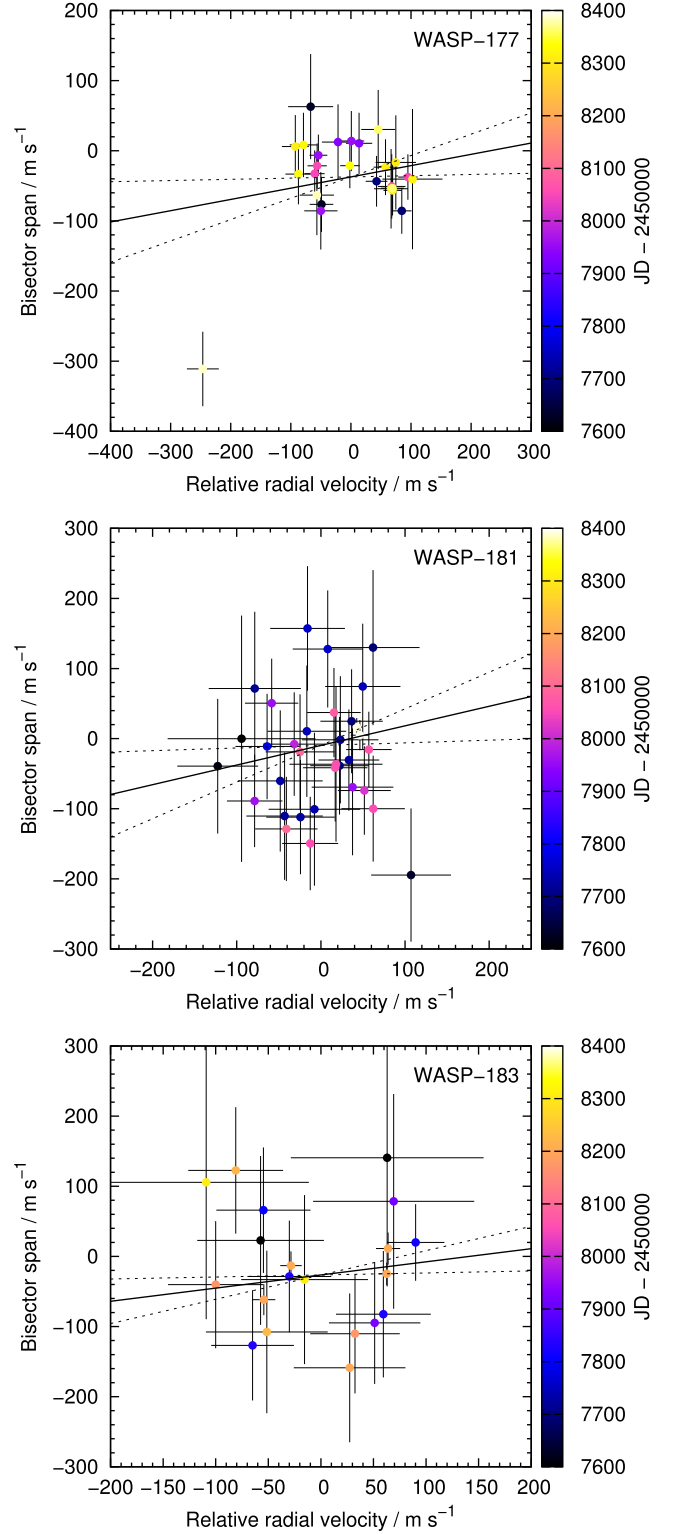
Figure 4. Radial velocity measurements plotted against line bisector spans. There is no strong correlation between the two, thus ruling out transit mimics. Solid lines are the linear best fit to the data. The dotted lines show the 1σ uncertainty limits on the fit.

Figure 5. Isochrones (solid/blue) and evolution tracks (dot–dashed/red) output by BAGEMASS for each of the planets we present with the corresponding isochrone age and mass (labelled).

Collier Cameron et al. (2007) and Anderson et al. (2015a). We modelled the transit light curves using the models of Mandel & Agol (2002) with the four parameter limb-darkening law of Claret (2000, 2004).

In brief, the models were initialized using the period, P, epoch, T_0, transit depth, $(R_p/R_s)^2$, transit duration, T_{14}, and i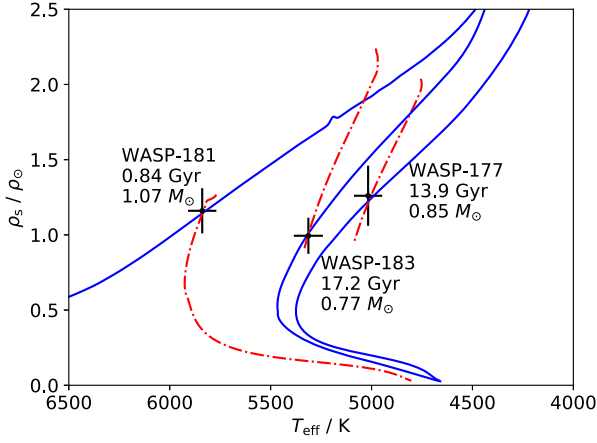mpact parameter, b, output by the BLS search of each discovery light curve. The spectroscopic stellar effective temperature, T_{eff}, and metallicity, [Fe/H], were used initially to estimate the stellar mass using the updated Torres mass calibration by Southworth (2011). To explore the effect of limb darkening we extracted tables of limb-darkening parameters in each photometric band used for each star. They were extracted for a range of effective temperatures while keeping the stellar metallicity and surface gravity constant. The values used were perturbed during the MCMC via T_{L-D}, the 'limb-darkening temperature', which has a mean and standard deviation corresponding to the spectroscopic T_{eff} and its uncertainty.

At each step of the MCMC each of these values are perturbed and the models are re-fit. These new proposed parameters are then accepted if the χ^2 of the fit is better or accepted with a probability proportional to $\exp(-\Delta\chi^2)$ if the χ^2 of the fit is worse.

In the final MCMCs, in place of using the Torres relation to determine a mass, we provided the value given by BAGEMASS. The code then drew values at each step from a Gaussian with a mean and standard deviation given by the value and its uncertainty, respectively. Due to the lack of good-quality follow-up photometry we imposed a similar prior on the radius of the star WASP-183 using the Gaia parallax. Lacking a complete, good-quality follow-up light curve can lead to a poor determination of, ΔF, T_{14}, and b which we use to calculate the R_*/a. This in turn results in a poorer determination of R_*, R_p and other parameters that depend upon them.

In this way we also explored models allowing for eccentric orbits and the potential for linear drifts in the RVs. There was no strong evidence supporting either scenario so we present the system solutions corresponding to circular orbits (Anderson et al. 2012) with no trends due to unseen companions. The parameters derived by these fits can be found in the lower part of Table 3.

3.3 Rotational modulation

We checked the WASP light curves of the three stars for rotational modulation that could be caused by star spots using the method

Table 2. Periodogram analysis for WASP light curves of WASP-177.

WASP Inst.	Dates JD-2450000	Period P_{rot} (d)	Amp (mag)	FAP	Notes
North	4656–4767	7.569	0.005	0.0017	P/2
North	5026–5131	7.528	0.006	<0.0001	P/2
North	5387–5498	14.860	0.004	<0.0001	
South	4622–4764	14.330	0.005	0.0007	
South	4984–5129	7.456	0.006	<0.0001	P/2

described by Maxted et al. (2011). The transits were fit with a simple model and removed. We performed the search over 16384 frequencies ranging from 0 to 1 cycles d^{-1}. Due to the limited lifetime and variable distribution of star spots this modulation is not expected to be coherent over long periods of time. As such, we modelled each season of data from each camera individually. WASP-181 and WASP-183 show no significant modulation, with an upper limit on the amplitude of 2- and 3-mmag, respectively.

However, WASP-177 was found to exhibit modulation consistent with a rotational period, $P_{rot} = 14.86 \pm 0.14$ d and amplitude of 5 ± 1 mmag. The results of this analysis for each camera and season of data are shown in Table 2. Fig. 6 shows the periodograms of the fits and the discovery light curves phase-folded on the corresponding period of modulation. Three of the data sets exhibit $P_{rot} \sim 7$ d while the other two exhibit $P_{rot} \sim 14$ d. We interpret the ~ 7 d signals as a harmonic of the longer ~ 14 d signal as it is more easy for multiple active regions to produce a ~ 7 d signal when the true period is ~ 14 d than vice versa. Using this rotational period and our value for the stellar radius we find a stellar rotational velocity of, $v_* = 2.9 \pm 0.2$ km s^{-1}. When compared to the projected equatorial spin velocity we find a stellar inclination to our line of sight of $38 \pm 25°$ which suggests that WASP-177 b could be quite mis-aligned.

4 DISCUSSION

Our joint analysis shows that in this ensemble we have two large sub-Jupiter mass planets: WASP-177 b (~ 0.5 M_{Jup}, ~ 1.6 R_{Jup}) and WASP-183 b (~ 0.5 M_{Jup}, ~ 1.5 R_{Jup}) orbiting old stars. The third planet, WASP-181 b, is a large Saturn mass planet (~ 0.3 M_{Jup}, ~ 1.2 R_{Jup}). According to the analysis with BAGEMASS, WASP-177, and WASP-183 are both at the latter end of the main sequence explaining their slightly larger radii for stars of their spectral class; a 9.7 ± 3.9 Gyr K2 and 14.9 ± 1.7 Gyr G9/K0, respectively. WASP-183 is particularly noteworthy as its advanced age makes it one of the oldest stars known to host a transiting planet (see Fig. 7). Though, WASP-183 appears to be subject to the K-dwarf radius anomaly, making this determination less clear. Meanwhile, WASP-181 is a relatively young, standard example of a G2 star.

We compared the stellar radii derived from our MCMC to those we can calculate using the Gaia DR2 parallaxes (Gaia Collaboration 2018; Luri et al. 2018), with the correction from Stassun & Torres (2018), and stellar angular radii from the infra-red flux fitting method (IRFM) these radii, with reddening accounted for by the use of dust maps (Schlafly & Finkbeiner 2011) . We find good agreement and present a summary in Table 4.

All three planets occupy the upper edge of the mass–radius distribution, seen in Fig 8. WASP-181 b is amongst the group of the largest planets for an object of its mass. While its mass is not as well determined as the other two, further HARPS observations will help to refine this. WASP-177 b and WASP-183 b do lie above the bulk of the distribution, especially when compared to other

Table 3. System parameters.

Parameter	Symbol (Unit)	WASP-177	WASP-181	WASP-183
1SWASP ID	−	J221911.19−015004.7	J014710.37+030759.0	J105509.36−004413.7
Right ascension	(h:m:s)	22:19:11.19	01:47:10.37	10:55:09.36
Declination	(°:′:″)	−01:50:04.7	+ 03:07:59.0	−00:44:13.7
V magnitude	−	12.58	12.91	12.76
Spectral type[a]	−	K2	G2	G9/K0
Stellar effective temperature	$T_{\rm eff}$ (K)	5017 ± 70	5839 ± 70	5313 ± 72
Stellar surface gravity	$\log (g)$ (cgs)	4.49 ± 0.07	4.38 ± 0.08	4.25 ± 0.09
Stellar metallicity	[Fe/H] (dex)	0.25 ± 0.04	0.09 ± 0.04	-0.31 ± 0.04
Projected equatorial spin velocity	$V_* \sin I_*$ (km s^{-1})	1.8 ± 1.0	3.3 ± 0.9	1.0 ± 1.0
Stellar macro-turbulent velocity[b]	$V_{\rm mac}$ (km s^{-1})	2.7	3.3	2.8
Stellar age	(Gyr)	9.7 ± 3.9	2.5 ± 1.7	14.9 ± 1.7
Distance[c]	(pc)	178 ± 2	443 ± 8	328 ± 4
Period	P (d)	$3.071\,722 \pm 0.000\,001$	$4.519\,5064 \pm 0.000\,0034$	$4.111\,7771 \pm 0.000\,0051$
Transit epoch	$T_0 - 2450000$	$7994.37140 \pm 0.000\,28$	7747.66681 ± 0.00035	7796.1845 ± 0.0024
Transit duration	T_{14} (d)	0.0672 ± 0.0013	0.1277 ± 0.0015	0.084 ± 0.005
Scaled semimajor axis	a/R_s	$9.61^{+0.42}_{-0.53}$	12.09 ± 0.54	11.44 ± 0.54
Transit depth	$(R_{\rm p}/R_{\rm s})^2$	$0.0185^{+0.0035}_{-0.0014}$	0.01590 ± 0.00038	$0.0226^{+0.0060}_{-0.0036}$
Impact parameter	b	$0.980^{+0.092}_{-0.060}$	$0.34^{+0.10}_{-0.15}$	$0.916^{+0.163}_{-0.091}$
Orbital inclination	i (°)	$84.14^{+0.66}_{-0.83}$	$88.38^{+0.76}_{-0.59}$	$85.37^{+0.61}_{-0.88}$
Systemic velocity	γ (kms^{-1})	-7.1434 ± 0.0041	-8.5489 ± 0.0072	68.709 ± 0.012
Semiamplitude	K_1 (ms^{-1})	77.3 ± 5.2	35.7 ± 3.9	74.8 ± 6.6
Semimajor axis	a (au)	0.03957 ± 0.00058	0.05427 ± 0.00069	0.04632 ± 0.00075
Stellar mass	$M_{\rm s}$ ($M_\odot$)	0.876 ± 0.038	1.04 ± 0.04	0.784 ± 0.038
Stellar radius	$R_{\rm s}$ ($R_\odot$)	0.885 ± 0.046	0.965 ± 0.043	0.871 ± 0.038
Stellar density	$\rho_{\rm s}$ ($\rho_\odot$)	$1.26^{+0.23}_{-0.15}$	1.16 ± 0.15	1.19 ± 0.17
Stellar surface gravity	$\log (g_s)$ (cgs)	$4.486^{+0.049}_{-0.037}$	4.487 ± 0.039	4.452 ± 0.043
Limb-darkening temperature	$T_{\rm L\text{-}D}$ (K)	5012 ± 69	5835 ± 70	5313 ± 72
Stellar metallicity	[Fe/H]	0 ± 0	0 ± 0	0 ± 0
Planet mass	$M_{\rm p}$ ($M_{\rm Jup}$)	0.508 ± 0.038	0.299 ± 0.034	0.502 ± 0.047
Planet radius	$R_{\rm p}$ ($R_{\rm Jup}$)	$1.58^{+0.66}_{-0.36}$	$1.184^{+0.071}_{-0.059}$	$1.47^{+0.94}_{-0.33}$
Planet density	$\rho_{\rm p}$ ($\rho_{\rm Jup}$)	$0.130^{+0.153}_{-0.085}$	0.179 ± 0.033	$0.16^{+0.18}_{-0.12}$
Planet surface	$\log (g_{\rm p})$ (cgs)	$2.67^{+0.22}_{-0.31}$	2.686 ± 0.065	$2.72^{+0.22}_{-0.43}$
Planet equilibrium temperature[d]	$T_{\rm eq}$ (K)	1142 ± 32	1186^{+32}_{-26}	1111 ± 30

[a]Spectral type estimated by comparison of $T_{\rm eff}$ to the table in Gray (2008).
[b]Derived via the method of Doyle et al. (2014).
[c]From Gaia DR2 Gaia Collaboration (2016, 2018) and Luri et al. (2018).
[d]Assuming 0 albedo and complete redistribution of heat.

objects with mass determinations of 10 per cent precision or better. However, it is difficult to say how exceptional they are as a precise radius determination has proven difficult for them both. The transit of WASP-177 b is grazing and the transit of WASP-183 b, in addition to being grazing, lacks a full high-precision follow-up light curve to refine the transit shape. We anticipate that *TESS* observations could soon solve the latter problem; the long cadence data would capture roughly 24 in transit points with a predicted precision from the *ticgen* tool of better than 1000 ppm in each 30 min observation.

We used the values derived for planet equilibrium temperature, $T_{\rm eq}$, and surface gravity, g, along with Boltzmann's constant, k, and the atmospheric mean molecular mass, μ, to estimate the scale heights, H, of these planets as:

$$H = \frac{kT_{\rm eq}}{g\mu} \qquad (1)$$

assuming an isothermal, hydrogen dominated atmosphere. The resulting scale heights were; 790 ± 320 km, 770 ± 200 km, 696 ± 464 km for WASP-177 b, WASP-181 b and WASP-183 b,

respectively. These translate to transit depth variations of just under 300 ppm for WASP-177 and WASP-181 and ∼300 ppm for WASP-183. If we account for the *K*-band flux and scale in the same way as Anderson et al. (2017), we get atmospheric signals of; 70, 41, and 60. In reality, we can expect this metric to be an overestimate of detectability for WASP-177 b and WASP-183 b as the grazing nature of their transits reduces the impact of the atmospheric signal further. For comparison we used the same metric on other planets with atmospheric detections: water has been detected in the atmospheres of both WASP-12 b (Kreidberg et al. 2015; signal ∼93) and WASP-43 b (Kreidberg et al. 2014; signal ∼74); titanium oxide has been detected in the atmosphere of WASP-19 b (Sedaghati et al. 2017; signal ∼83); sodium and potassium have both been detected in the atmosphere of WASP-103 b (Lendl et al. 2017; signal ∼37). While not ideal targets, this suggests such detections may be possible.

Investigation into any eccentricity or long-period massive companions in these systems has not yielded anything convincing. All of the orbits are circular, with the 2σ upper limits quoted in Table 3. As for long-term trends, WASP-177 shows the possibility of a very
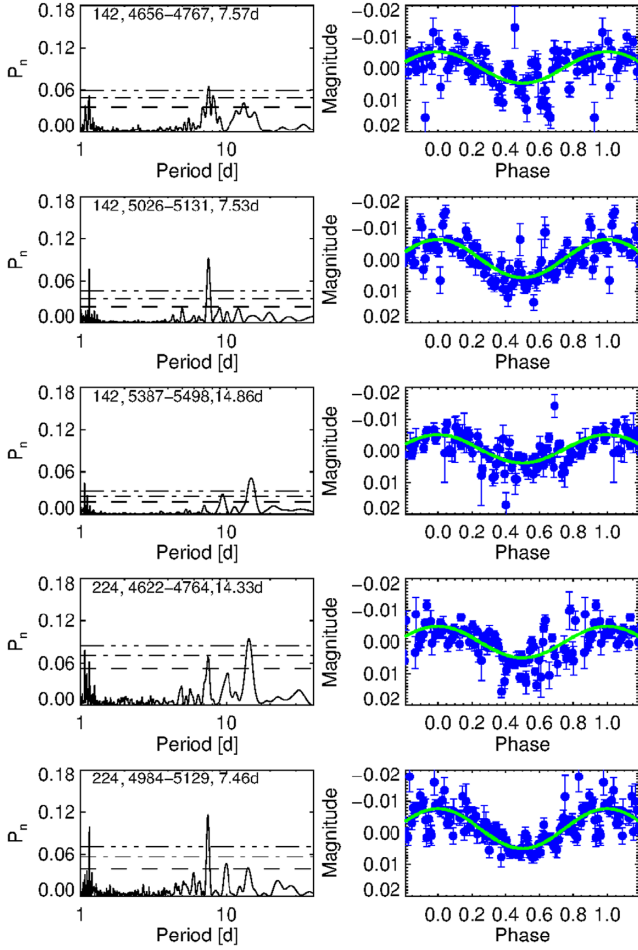
Figure 6. *Left*: Periodograms of the WASP light curves of WASP-177. Each is labelled with the corresponding camera ID, dates of the observation period (in JD-2450000) and period of the most significant signal. Horizontal lines indicate false-alarm probability levels of 0.1, 0.01, and 0.001. *Right*: Light curves folded on the most significant detected period.

low significance ($\sim 1.5\sigma$) drift with $\delta\gamma/\delta t$ of $(-2.4 \pm 1.6) \times 10^{-5}$ km^{-1} s^{-1} d. Neither WASP-181 nor WASP-183 show significant drifts with $\delta\gamma/\delta t$ of $(1.2 \pm 4.0) \times 10^{-5}$ km^{-1} s^{-1} d and $(-1.9 \pm 5.1) \times 10^{-5}$ km^{-1} s^{-1} d, respectively.

Finally, these systems do present interesting targets for the investigation of the observed spin–orbit mis-alignment distribution (Albrecht et al. 2012; Anderson et al. 2015b). All of the stellar hosts fall into the 'cool' regime of Albrecht et al. (2012) and despite their short periods have scaled semimajor axes, a/R_*, above 8. They are therefore above the empirical boundary noted by Dai & Winn (2017) as the transition region where systems with cooler stars show more tendency to be mis-aligned. Since the study in 2017 the number of systems with obliquity measurements has increased. Most of the cool-star systems with a/R_* above 8 are well aligned, see Fig 9.

We estimated the alignment time-scale for each system using equation (4) of Albrecht et al. (2012) as was done for WASP-117 (Lendl et al. 2014). These time-scales, along with the mass of the convective zone, M_{cz}, are shown in Table 5 . In each case, the time-scale for realignment is much longer than the ages of the systems. Therefore, we would expect the initial state of alignment of the systems to have been preserved. We have estimated the inclination of WASP-177 to be $38 \pm 25°$ and so may expect it to join only
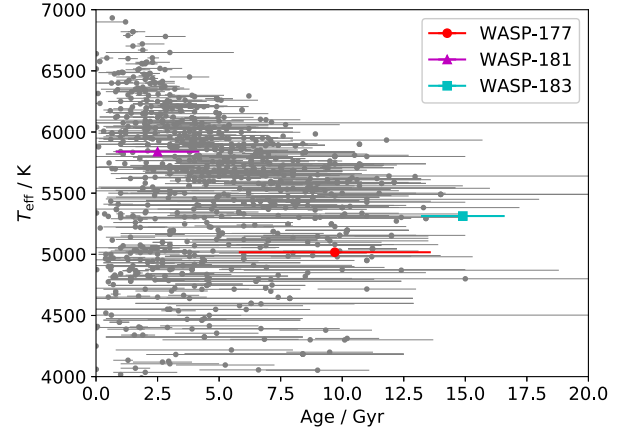
Figure 7. Age distribution for known exoplanet hosts with published uncertainties (grey) and planets presented in this paper (see legend). WASP-183 appears to be particularly old amongst planet hosts. However, we note it is unphysically old and so caution that this determination may be in part due to the K-dwarf radius anomaly. (Data from exoplanet.eu.).

Table 4. Comparison of stellar radii output by the MCMC analysis with radii derived from Gaia DR2.

| Radius source	WASP-177	WASP-181	WASP-183
MCMC	0.885 ± 0.046	0.965 ± 0.043	0.871 ± 0.038
Gaia parallax + IRFM (Corrected)	0.80 ± 0.04	0.97 ± 0.06	0.87 ± 0.04
Gaia parallax + IRFM (Uncorrected)	0.81 ± 0.04	1.01 ± 0.05	0.89 ± 0.04
Reddening	0.072	0.023	0.04
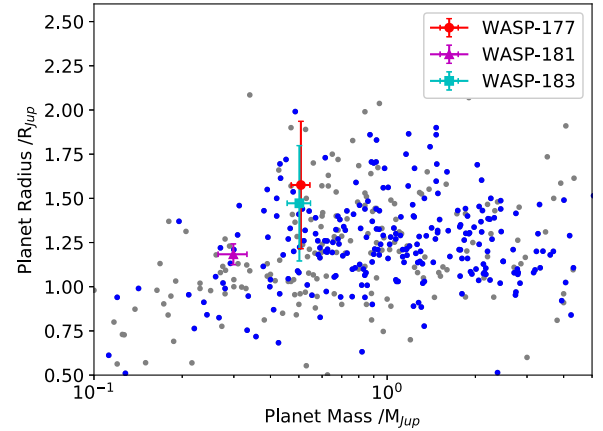
Figure 8. Mass–radius distribution for transiting planets. Planets with masses determined to better than 10 per cent precision are plotted in blue, otherwise the symbols are grey. WASP-177 b, WASP-181 b, and WASP-183 b have been plotted with their error bars. Each is close to the upper most part of the distribution. WASP-177 b is in an area particularly sparsely populated by planets with well determined masses. (Prepared using data collated from the TEPCat; Southworth 2011.).

12 systems with $a/R_* < 15$ that show mis-alignment this makes it a potentially important diagnostic in determining the factors that cause or preserve mis-alignment.

We calculate that the amplitude of the RM effect will be greatest for WASP-181 at ~ 50 ms^{-1}. The effect should also be detectable
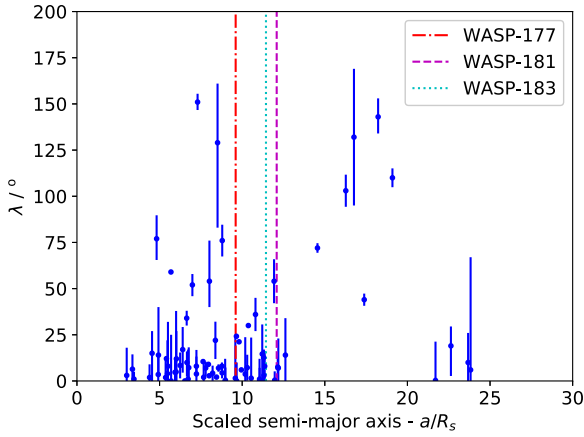
Figure 9. Distribution of planets with measured spin–orbit angles with cool host stars. WASP-177, WASP-181, and WASP-183 are all cool stars by this definition and the planets lie in the region where mis-alignment is often said to become more common. WASP-177 shows signs of being misaligned and so may be an interesting diagnostic in this region. (Prepared using data collated from the TEPCat; Southworth 2011.).

Table 5. Convective zone masses and estimated time-scales for realignment of systems in this paper.

Star	$M_{cz}{}^a$ (M$_\odot$)	τ (Gyr)
WASP-177	$10^{-1.3}$	120
WASP-181	$10^{-1.7}$	7500
WASP-183	$10^{-1.4}$	200

^{a}Dervied from Pinsonneault, DePoy & Coffee (2001).

for WASP-177 and WASP-183 despite their more grazing transits, with an amplitude of $\sim$10 ms^{-1}.

5 CONCLUSIONS

We have presented the discovery of three transiting exoplanets from the WASP survey; WASP-177 b ($\sim$0.5 M$_{Jup}$, $\sim$1.6 R$_{Jup}$), WASP-181 b ($\sim$0.3 M$_{Jup}$, $\sim$1.2 R$_{Jup}$), and WASP-183 b ($\sim$0.5 M$_{Jup}$, $\sim$1.5 R$_{Jup}$). They all occupy the upper region of the mass–radius distribution for hot gas-giant planets but do not present exceptional targets for transmission spectroscopy. However, regarding the investigation of system spin–orbit alignment they do occupy an under investigated range of a/R_* and so could act as good probes of tidal realignment time-scales.

REFERENCES

Albrecht S. et al., 2012, ApJ, 757, 18
Anderson D. R. et al., 2012, MNRAS, 422, 1988
Anderson D. R. et al., 2015a, A&A, 575, A61
Anderson D. R. et al., 2015b, ApJ, 800, L9
Anderson D. R. et al., 2017, A&A, 604, A110
Armitage P. J., 2013, Astrophysics of Planet Formation. Cambridge University Press, Cambridge
Barkaoui K., et al., 2018, AJ, 157, 43
Birkby J. L., de Kok R. J., Brogi M., de Mooij E. J. W., Schwarz H., Albrecht S., Snellen I. A. G., 2013, MNRAS, 436, L35
Blanco-Cuaresma S. et al., 2016, in Feiden G. A., ed., 19th Cambridge Workshop on Cool Stars, Stellar Systems, and the Sun (CS19), Rymdstyrelsen, Sweden. p. 22
Blanco-Cuaresma S. et al., 2017, in Arribas S., Alonso-Herrero A., Figueras F., Hernándey-Monteagudo, Sánchez-Lavega, Pérez-Hoyos, eds, Highlights on Spanish Astrophysics IX, Proceedings of the XII Scientific Meeting of the Spanish Astronomical Society held on July 18-22, 2016, in Bilbao, Spain, p. 334
Blanco-Cuaresma S., Soubiran C., Jofré P., Heiter U., 2014a, A&A, 566, A98
Blanco-Cuaresma S., Soubiran C., Heiter U., Jofré P., 2014b, A&A, 569, A111
Brogi M., de Kok R. J., Albrecht S., Snellen I. A. G., Birkby J. L., Schwarz H., 2016, ApJ, 817, 106
Claret A., 2000, A&A, 363, 1081
Claret A., 2004, A&A, 428, 1001
Collier Cameron A. et al., 2006, MNRAS, 373, 799
Collier Cameron A. et al., 2007, MNRAS, 380, 1230
Dai F., Winn J. N., 2017, AJ, 153, 205
de Kok R. J., Brogi M., Snellen I. A. G., Birkby J., Albrecht S., de Mooij E. J. W., 2013, A&A, 554, A82
Doyle A. P., Davies G. R., Smalley B., Chaplin W. J., Elsworth Y., 2014, MNRAS, 444, 3592
Fabrycky D., Tremaine S., 2007, ApJ, 669, 1298
Gaia Collaboration, 2016, A&A, 595, A1
Gaia Collaboration, 2018, A&A, 616, A1
Giles H. A. C. et al., 2018a, MNRAS, 475, 1809
Giles H. A. C. et al., 2018b, A&A, 615, L13
Gillon M. et al., 2011, A&A, 533, A88
Gillon M. et al., 2017, Nature, 542, 456
Goldreich P., Tremaine S., 1980, ApJ, 241, 425
Gray D. F., 2008, The Observation and Analysis of Stellar Photospheres. Cambridge Univ. Press, Cambridge
Gray R. O., Corbally C. J., 1994, AJ, 107, 742
Gustafsson B., Edvardsson B., Eriksson K., Jørgensen U. G., Nordlund Å., Plez B., 2008, A&A, 486, 951
Heiter U., Jofré P., Gustafsson B., Korn A. J., Soubiran C., Thévenin F., 2015, A&A, 582, A49
Hoeijmakers H. J. et al., 2018, Nature, 560, 453
Jehin E. et al., 2011, The Messenger, 145, 2
Jofré P. et al., 2014, A&A, 564, A133
Kreidberg L. et al., 2014, ApJ, 793, L27
Kreidberg L. et al., 2015, ApJ, 814, 66
Kupka F., Dubernet M.-L., VAMDC Collaboration, 2011, Balt. Astron., 20, 503

Lendl M. et al., 2012, A&A, 544, A72

Lendl M. et al., 2014, A&A, 568, A81

Lendl M., Cubillos P. E., Hagelberg J., Müller A., Juvan I., Fossati L., 2017, A&A, 606, A18

Luri X. et al., 2018, A&A, 616, A9

Mandel K., Agol E., 2002, ApJ, 580, L171

Marzari F., Nelson A. F., 2009, ApJ, 705, 1575

Maxted P. F. L. et al., 2011, PASP, 123, 547

Maxted P. F. L., Serenelli A. M., Southworth J., 2015, A&A, 575, A36

Mazeh T., Perets H. B., McQuillan A., Goldstein E. S., 2015, ApJ, 801, 3

McLaughlin D. B., 1924, ApJ, 60, 22

Pepe F. et al., 2002, The Messenger , 110, 9

Pinsonneault M. H., DePoy D. L., Coffee M., 2001, ApJ, 556, L59

Pollacco D. L. et al., 2006, PASP, 118, 1407

Queloz D. et al., 2000, A&A, 354, 99

Rasio F. A., Ford E. B., 1996, Science, 274, 954

Rossiter R. A., 1924, ApJ, 60, 15

Schlafly E. F., Finkbeiner D. P., 2011, ApJ, 737, 103

Sedaghati E. et al., 2017, Nature, 549, 238

Southworth J., 2011, MNRAS, 417, 2166

Spada F., Demarque P., Kim Y.-C., Sills A., 2013, ApJ, 776, 87

Stassun K. G., Torres G., 2018, ApJ, 862, 61

Triaud A. H. M. J. et al., 2010, A&A, 524, A25

Weidenschilling S. J., Marzari F., 1996, Nature, 384, 619

Wu Y., Murray N., 2003, ApJ, 589, 605

Wyttenbach A. et al., 2017, A&A, 602, A36

Xiang-Gruess M., Kroupa P., 2017, MNRAS, 471, 2334

SUPPORTING INFORMATION

Supplementary data are available at *MNRAS* online.

Table A1. Data from WASP.

Table A2. Data from Trappist.

Table A3. RV data.

Table A4. Data from Euler.

Please note: Oxford University Press is not responsible for the content or functionality of any supporting materials supplied by the authors. Any queries (other than missing material) should be directed to the corresponding author for the article.

APPENDIX A: ONLINE DATA

We include the data we used in this paper as online material. Examples of the tables are shown here.

Table A1. Data from WASP.

BJD-2450000	Diff. magnitude	Mag. error	Target
5026.54902768	− 0.002 549 00	0.019 491 00	WASP-177
5026.54946749	0.022 430 00	0.019 577 00	WASP-177
5026.55550916	− 0.003 155 00	0.019 265 00	WASP-177
5026.55596055	− 0.002 109 00	0.018 918 00	WASP-177
5026.56091425	0.023 018 00	0.018 927 00	WASP-177
5026.56135407	− 0.010 706 00	0.018 290 00	WASP-177
5026.56629620	− 0.018 209 00	0.018 365 00	WASP-177
5026.56673601	− 0.030 871 00	0.017 690 00	WASP-177
5026.57268508	− 0.024 534 00	0.017 800 0	WASP-177
5026.57312490	− 0.007 008 00	0.018 186 00	WASP-177

Table A2. Data from Trappist.

BJD-2450000	Dif. Mag.	Mag. error	Filter	Target
7960.51599185	− 0.00760377	− 0.00345472	I + z	WASP-177
7960.51636185	− 0.00029799	− 0.00344426	I + z	WASP-177
7960.51664185	0.00210904	− 0.00344268	I + z	WASP-177
7960.51691185	− 0.00560489	− 0.00344076	I + z	WASP-177
7960.51718185	− 0.00165321	− 0.00342985	I + z	WASP-177
7960.51754185	− 0.00448940	− 0.00342637	I + z	WASP-177
7960.51782185	− 0.00682232	− 0.00342797	I + z	WASP-177
7960.51809185	0.00938183	− 0.00343320	I + z	WASP-177
7960.51836185	− 0.00237813	− 0.00343161	I + z	WASP-177
7960.51863185	− 0.00132194	− 0.00342244	I + z	WASP-177

Table A3. RV data.

JD-2450000	RV (km s^{-1})	RV error	Instrument	Target
7626.633110	−7.192 43	0.019 63	CORALIE	WASP-177
7629.687997	−7.210 44	0.037 48	CORALIE	WASP-177
7689.581199	−7.058 73	0.016 34	CORALIE	WASP-177
7695.567558	−7.100 68	0.018 12	CORALIE	WASP-177
7933.845373	−7.164 82	0.026 86	CORALIE	WASP-177
7937.771917	−7.129 78	0.021 80	CORALIE	WASP-177
7952.880188	−7.142 80	0.021 44	CORALIE	WASP-177
7954.787481	−7.197 49	0.014 73	CORALIE	WASP-177
7961.703754	−7.193 47	0.027 63	CORALIE	WASP-177
8047.604223	−7.203 69	0.016 60	CORALIE	WASP-177

Table A4. Data from Euler.

BJD-2450000	Dif. Mag.	Mag. error	X-pos (pix)	Y-pos (pix)	Airmass	FWHM (pix)	Sky Bkg.	Exp. time (s)	Filter (d)	Object
8046.53876846	0.000 345 78	0.003 593 81	1070.950	571.822	1.1298	9.369	0.869	110	B	WASP-177
8046.54029585	0.000 372 22	0.003 582 08	1086.396	562.842	1.1289	7.076	0.903	110	B	WASP-177
8046.54281198	− 0.8042	0.002 135 08	1085.203	562.140	1.1279	7.496	2.5836	300	B	WASP-177
8046.54652188	− 0.000 240 34	0.002 134 11	1086.544	558.005	1.1267	7.632	2.4149	300	B	WASP-177
8046.55014519	0.000 317 79	0.002 135 39	1086.429	558.463	1.1262	7.980	2.3836	300	B	WASP-177
8046.55443872	0.003 131 22	0.001 842 58	1085.948	555.787	1.1264	7.832	3.2365	400	B	WASP-177
8046.55920903	0.003 632 11	0.001 844 63	1084.985	556.119	1.1274	7.832	3.4133	400	B	WASP-177
8046.56407976	0.002 798 18	0.001 851 39	1087.955	557.254	1.1296	7.928	3.4343	400	B	WASP-177
8046.56884813	0.006 396 43	0.001 861 26	1087.783	558.089	1.1326	9.099	3.9564	400	B	WASP-177
8046.57371742	0.009 385 02	0.001 856 10	1089.022	557.002	1.1369	7.880	3.5795	400	B	WASP-177

This paper has been typeset from a TEX/LATEX file prepared by the author.